

A Novel Time Reversal Based Microwave Imaging System

Amin Tayebi^{1, 2, *}, Pavel Roy Paladhi¹, Lalita Udpa¹, and Satish Udpa¹

Abstract—This paper presents an alternate microwave imaging system that greatly reduces design and operation complexities compared to traditional imaging systems. At the heart of this novel system lies an electronically reconfigurable beam-scanning reflectarray antenna. The high tuning capability of the reflectarray provides us a broad steering range of $\pm 60^\circ$. The beam is steered across this range and the scattered field is recorded. The collected data are used for image reconstruction by means of the time reversal signal processing technique. Experimental results of the detection of various dielectric targets are presented.

1. INTRODUCTION

The applications of microwave imaging range from breast cancer detection [1] to machine vision and robotics [2]. Microwave imaging has gained special attention in the field of medical imaging due to the continued increase in breast cancer diagnoses. In 2015, in the United States, it was estimated that 292,130 women were diagnosed with invasive or carcinoma in situ types of breast cancer [3]. Thus, there is an urgent need to develop a more reliable and effective detection system. Microwave imaging is known to be a promising candidate for early breast cancer detection [4] due to its ability to differentiate between the high contrast in dielectric properties of malignant and healthy breast tissues. Another area in which microwave imaging has been widely applied is in the non-destructive testing (NDT) of composite materials, where traditional approaches fail. A detailed overview and discussion of the advances in microwave NDT can be found in [5].

A new prototype for an active microwave imaging system is presented in this paper. The key feature of the system is the utilization of a tunable reflectarray antenna to scan the region of interest (ROI). The collected scattered field is then conveniently used in a time reversal based algorithm to detect scatterers. This is an alternative to conventional microwave imaging systems with significant advantages. A traditional tomographic setup needs an array of costly transceivers to be placed all around the object [6–11]. This requires complicated circuitry and results in a high production cost of the system. The reflectarray paired with a single source greatly alleviates both of these issues. In addition, unlike conventional setups, this system is not constrained by the dimensions of the object. Therefore the inspection of large objects such as extended laminate structures and composite airplane wings becomes possible. Moreover, our system is scalable and has the potential for medical applications such as breast cancer detection. Not only can the system detect a tumor, the beam shaping capability of the reflectarray allows for the formation of pencil-shaped beams for therapy purposes. This work was inspired by [12, 13], where a system employing a deformable mirror for generating projections was investigated using a theoretical framework. This paper presents the implementation using the reflectarray instead of a mechanically conformable mirror. Details on the design of the proposed system and experimental results attained using a prototype are presented in this work.

The paper is organized as follows. The underlying principles of reflectarray antennas are briefly explained in Section 2. The unit cell of the utilized reflectarray is introduced and its tuning ability is

Received 24 January 2016, Accepted 23 February 2016, Scheduled 2 March 2016

* Corresponding author: Amin Tayebi (tayebiam@msu.edu).

¹ Department of Electrical and Computer Engineering, Michigan State University, East Lansing, MI 48824, USA. ² Department of Physics and Astronomy, Michigan State University, East Lansing, MI 48824, USA.

studied. Using this unit cell, a 10×10 array is fabricated. The high beam steering capability of the reflectarray is experimentally validated. Section 3 provides a brief summary of the principles of the time reversal symmetry and signal processing technique. Section 4 describes the experiments conducted using the imaging prototype. The results are provided and discussed. Section 5 includes some concluding remarks.

2. THE REFLECTARRAY ANTENNA

Reflectarray antennas are arrays of radiating elements illuminated by an external source. The elements of the array possess distinct radiation characteristics. The properties of the individual cells are determined in such a way that the field reflected from the surface of the array forms the desired radiation pattern. Thanks to microstrip technology, fabrication of these types of antennas is now straightforward and cost effective. The radiation characteristics of the unit element of microstrip reflectarrays depend heavily on their geometry and size. Microstrip reflectarrays of various geometries such as square patches, circular rings and cross dipoles are studied in [14]. An additional feature of versatility is added by dynamically altering the characteristics of the individual elements by electrical or mechanical means. This results in the so-called reconfigurable reflectarray antennas, where one can exploit features such as beam steering. Recent reviews on tunable and beam-scanning reflectarray antennas can be found in [15, 16].

The unit cell geometry of the beam-scanning reflectarray in our system consists of a square patch loaded with a square ring [17, 18]. The unit cell is depicted in Fig. 1. Here, tunability is achieved by using a single varactor diode that is connected between the ring and the patch. By varying the applied voltage, the capacitance value of the diode changes which in turn changes the resonating frequency of the structure. The parameters, g , d and ℓ are chosen so that the unit cell operates in the two distinct S and F frequency bands. However, it was found in [19] that the unit cell has a higher radiation efficiency in the F band. Therefore, for the purpose of this paper, we limit our operation to the F frequency band only.

In order to evaluate the tuning capabilities of the unit cell, a prototype was produced for measurement purposes. The unit cell was fabricated on a 1.575 mm thick RT/duroid 5880 substrate with dielectric constant of $\epsilon_r = 2.20$ and dissipation factor of $\tan \delta = 0.0009$. A GaAs hyperabrupt varactor diode (Aeroflex Metelics MG V100-20) with a dynamic range of 0.18–2.0 pF (corresponding to the voltage range 28–0.5 V) was connected between the ring and the patch. An F band waveguide was utilized in order to measure the reflection phase of the unit cell [20]. The fabricated unit cell was placed inside the waveguide and S parameters were measured. The reflection phase is the phase of S_{11} . The PEC boundaries of the waveguide effectively mimic the infinite periodic structure of the unit cell. This takes into account the mutual interaction between neighboring cells and therefore provides a realistic estimate of the behavior of the unit cell. Fig. 2 shows the measured reflection phase as a function of frequency for various voltage values. The figure demonstrates the high tuning ability of the unit cell over a frequency band from 5 to 6.25 GHz. A maximum phase range of 335° was observed at 5.30 GHz.

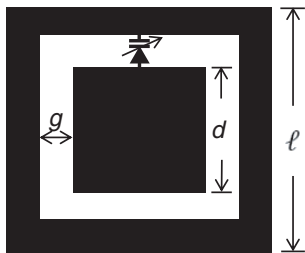


Figure 1. Geometry of the unit cell. The parameters are $g = 1$ mm, $d = 12$ mm and $\ell = 18$ mm.

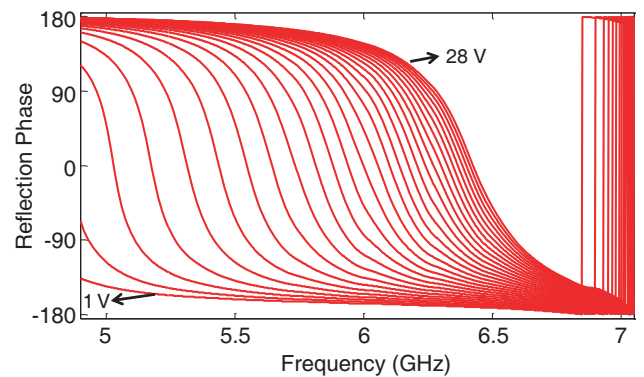


Figure 2. Measured reflection phase using an F band waveguide. The applied voltage range is 1 V to 28 V, with 1 V increments.

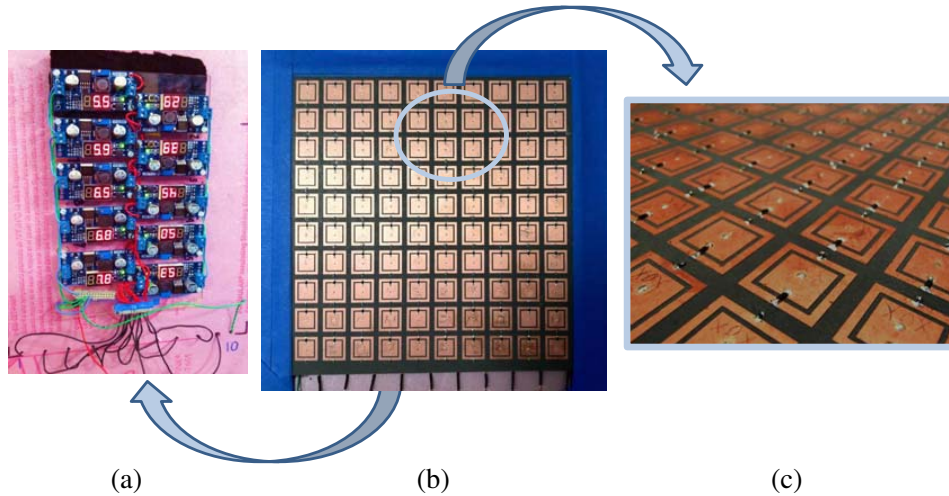


Figure 3. Reflectarray antenna: (a) shows back view with controller circuitry. (b), (c) show the front and the close up view of the reflectarray, respectively.

Using the designed unit cell, a 10×10 reflectarray antenna was fabricated. Neighboring unit cells were 4 mm apart corresponding to the final dimension of $220 \text{ mm} \times 220 \text{ mm}$ square array. Fig. 3 shows the front view and the biasing circuitry on the back of the array. In each column, all elements were connected to a single voltage regulator, having equal voltage. Therefore, all elements in a given column had the same reflection phase. This results in two dimensional beam steering in the plane normal to the surface of the reflectarray. In order to steer the beam into different directions, various voltage configurations were applied to the array. The radiation pattern was measured using an arch range [21] to perform bistatic measurements. Fig. 4 shows the steering of the main beam onto 0° , 30° , 45° and 60° at 6.10 GHz. Clearly, reversed order voltage configurations would result in beam steering into negative angles, therefore the array provides us a broad scanning range of $\pm 60^\circ$. This reflectarray is the main component of our prototype imaging system discussed in Section 4.

3. TIME REVERSAL SIGNAL PROCESSING

It is known that classical electromagnetic theory is invariant under the time reversal transformation. In order to see this, consider the electromagnetic wave equation describing the propagation of the electric field in a loss-less medium

$$\left(\nabla^2 - \frac{1}{c^2} \frac{\partial^2}{\partial t^2} \right) \vec{E}(\vec{r}, t) = 0, \quad (1)$$

where ∇ is the vector Laplacian operator, c the speed of light in the medium and $\vec{E}(\vec{r}, t)$ the electric field. Under the time reversal transformation, i.e., $t \rightarrow -t$, the wave Equation (1) stays invariant and holds its form. Consequently, if $\vec{E}(\vec{r}, t)$ is a solution to the equation, $\vec{E}(\vec{r}, -t)$ would be a solution as well. Notice, the symmetry is violated if the medium is lossy. This is because the presence of loss introduces a first order time derivative in Eq. (1), and hence the wave equation is no longer invariant under the time reversal transformation.

The time reversal symmetry has a significant practical implication. If one measures the electric field emitted from a source via an antenna array, time reverses the received signals and re-emits them back, the electric field focuses at the initial source of radiation. In a case where there are scatterers present in the medium, they act as secondary sources and the re-emitted time-reversed signals focus at the location of the scatterers. Therefore, this property can be successfully used as a reconstruction scheme in order to detect and locate scatterers in a medium. This approach is known as time reversal imaging and it has been vastly used as a powerful imaging technique. In [22] a new radar system utilizing time reversal imaging is introduced. It has been experimentally shown that the time-reversed signals focus on the target. Through-the-wall target localization has been demonstrated using the time reversal

MUSIC method in [23]. Time reversal microwave imaging with random configurations of transmitters or receivers is studied in [24]. In [25] the feasibility of microwave breast cancer detection using time reversal algorithms is investigated. Time reversal microwave techniques were also utilized for NDT of laminates and composite materials in [26]. The application of the time reversal symmetry is not limited to imaging however; in [27] time reversal is used for fault detection in wire networks.

In this work, time reversal imaging is the main reconstruction scheme used in order to detect and identify the location of scatterers. For various scatterer configurations, the scattered field is experimentally measured and stored. Time reversal focusing is then achieved using computer simulation. The measured scattered fields are reversed and plugged into an in-house finite difference time domain (FDTD) solver. The signals are backpropagated utilizing the software. The waves merge together at the exact location of the targets and hence detection is achieved. The details of the experimental setup and results are presented in the next section.

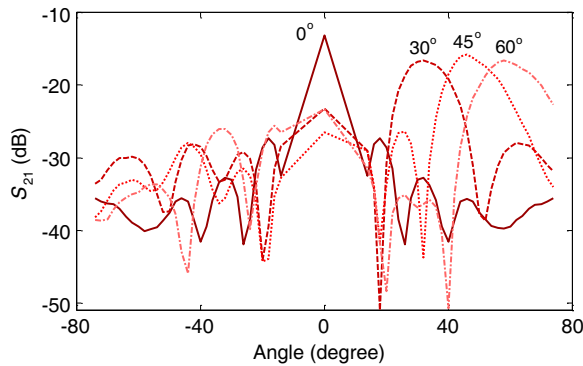


Figure 4. Beam steering at 6.10 GHz.

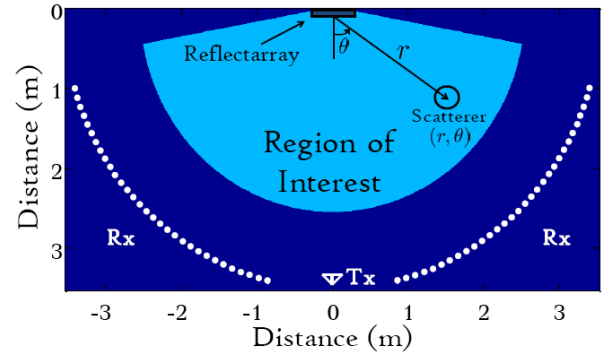


Figure 5. Schematic of the microwave imaging setup.

4. EXPERIMENTAL RESULTS

A prototype of the proposed microwave imaging system was built using the reflectarray antenna and the arch range at Michigan State University [21]. Fig. 5 depicts the schematic of the system. The reflectarray antenna, mounted on a Styrofoam sheet, was located at the center of the arch range, which has a radius of 3.53 m. The reflectarray is chosen to be the origin of the polar coordinate system used throughout the experiment (see Fig. 5). The line normal to the array corresponds to $\theta = 0$ and the curved arrow shows the direction in which θ increases. An H-1498 series broadband horn antenna was placed on the arch rail facing the reflectarray and was used as the source. A dielectric lens was placed in front of the antenna in order to create a focused plane wave beam. Moreover, the transmitter was aligned with the center of the reflectarray and the incident beam was directed to be perpendicular to the surface of the array. Both the array and the transmitter were kept stationary throughout the experiment. The reflectarray antenna steered the beam into different angles, sweeping the region of interest, and the scattered field was measured by a receiver antenna. An identical horn antenna was used as the receiver. The transmitter and the receiver were both connected to an Agilent E5071c network analyzer, calibrated from 1.5 GHz to 7.5 GHz with 1601 frequency points. The receiver antenna was moved along the arch rail in order to measure the transmission scattering parameter S_{21} . The white dots in Fig. 5 represent locations where a reading was taken. Measurements were taken every two degrees from $\theta = -74^\circ$, represented by the left-most dot, to $\theta = 74^\circ$, represented by the right-most dot. Due to the large size of the focusing lens of both the transmitter and the receiver, measurements could not be taken from $\theta = -14^\circ$ to $\theta = 14^\circ$. The measured signals at each position were calibrated using the response of the system. The system response was calculated in accordance to [21], by considering the canonical problem of scattering off a metal sphere.

For each angle at which the beam was steered, the background (free space) field was measured to be used as a reference. This reference was later subtracted from field measurements of different scatterer

configurations in order to obtain the respective scattered fields. Since the measurements were performed in the frequency domain, the resulting scattered field was Fourier transformed in order to get the time domain signal. Next, these signals were time reversed and re-radiated back using the FDTD simulation software. As explained in Section 3, the propagating time-reversed signals focus on the scatterers in the medium and hence detect and locate the targets. Similar to [26, 28], the electric field energy density (in units of $\frac{1}{2}\epsilon_0$) was calculated using the expression

$$W(\vec{r}) = \sum_{t=0}^T \left| \vec{E}(\vec{r}, t) \right|^2, \tag{2}$$

where \vec{E} is the electric field at point \vec{r} and time t , and T is the total simulation time. $W(\vec{r})$ can be interpreted as the accumulated energy at each point \vec{r} during backpropagation. It is important to mention that, in all experiments performed, the scattering objects were sufficiently tall so the problem was considered to be two dimensional. Also, the region of interest where the image is reconstructed is a 100-inch radius circular sector shown in Fig. 5. The area near the sources has been excluded from the ROI because of the high energy concentration and possible masking of target indications.

Two experiments were performed in order to demonstrate the feasibility of the approach. In the first experiment, the reflectarray was set to deflect the beam at the fixed angle of 45° . A cylindrical acetal (polyoxymethylene) with dielectric constant of 2.74 and dissipation factor of $\tan \delta = 0.006$ at room temperature was used as a target [29]. The cylinder had a diameter of 4 inches and a height of 12 inches and was located at $\theta = 45^\circ$. Measurements were taken of the cylinder placed at three different distances from the center of the array; 40, 60 and 80 inches. For each case, the energy image was reconstructed according to Eq. (2). Fig. 6 shows the reconstructed image without any further processing for the three different cases. As expected, the indication associated with the target is stretched out. This is because the measurements of the scattered field were not taken from all possible angles. This pattern was also observed in [24, 26]. The figure indicates that the intensity of the scattered field reduces as the object

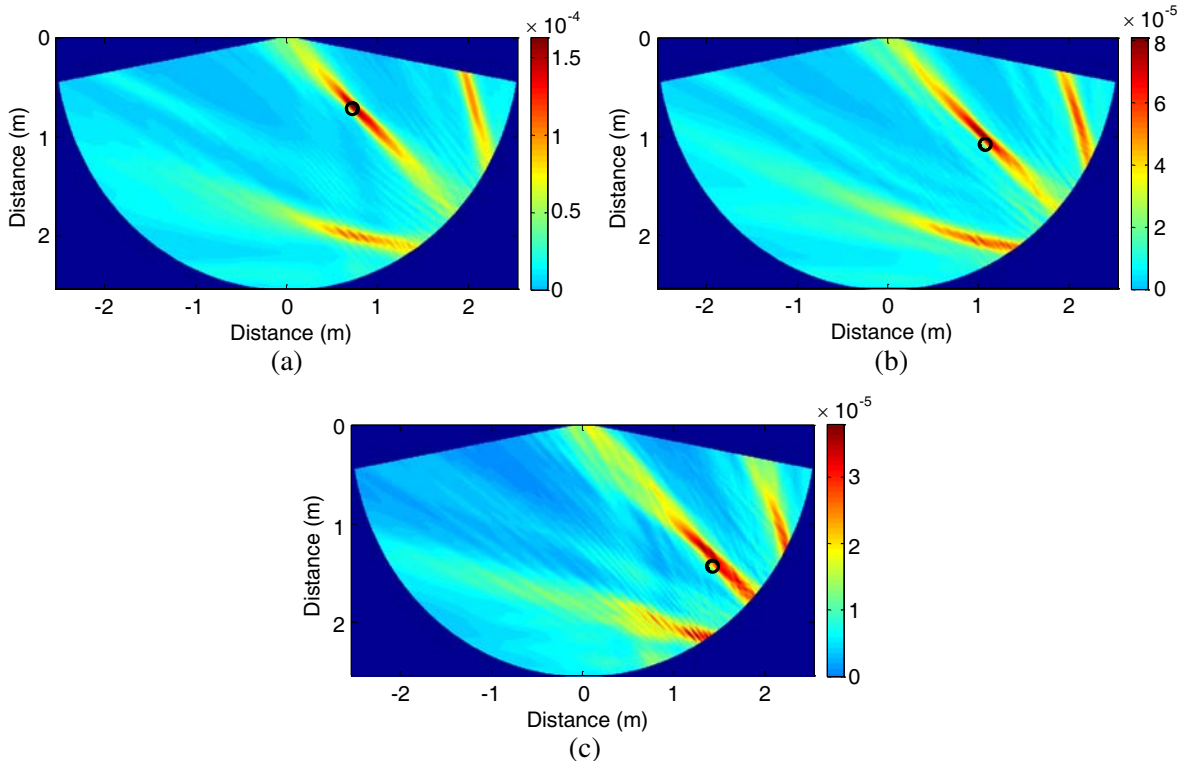


Figure 6. Experiment one. Energy image; the black circle corresponds to the actual position of the scatterer. (a) Target at 40 inches from the origin. (b) Target at 60 inches from the origin. (c) Target at 80 inches from the origin.

is placed farther away from the reflectarray antenna. This is due to path loss and divergence of the beam as the field propagates through space. The maximum intensity in Fig. 6(a), corresponding to the target 40 inches from the array, is almost an order of magnitude greater than the maximum intensity in Fig. 6(c), where the target is located 80 inches away from the array. The artifacts in the images are due to the limited bandwidth of the steered electric field.

In order to evaluate the accuracy of our system, it is assumed that the maximum intensity point in the image corresponds to the center of the cylindrical scatterer. Then the relative error in detection is defined as:

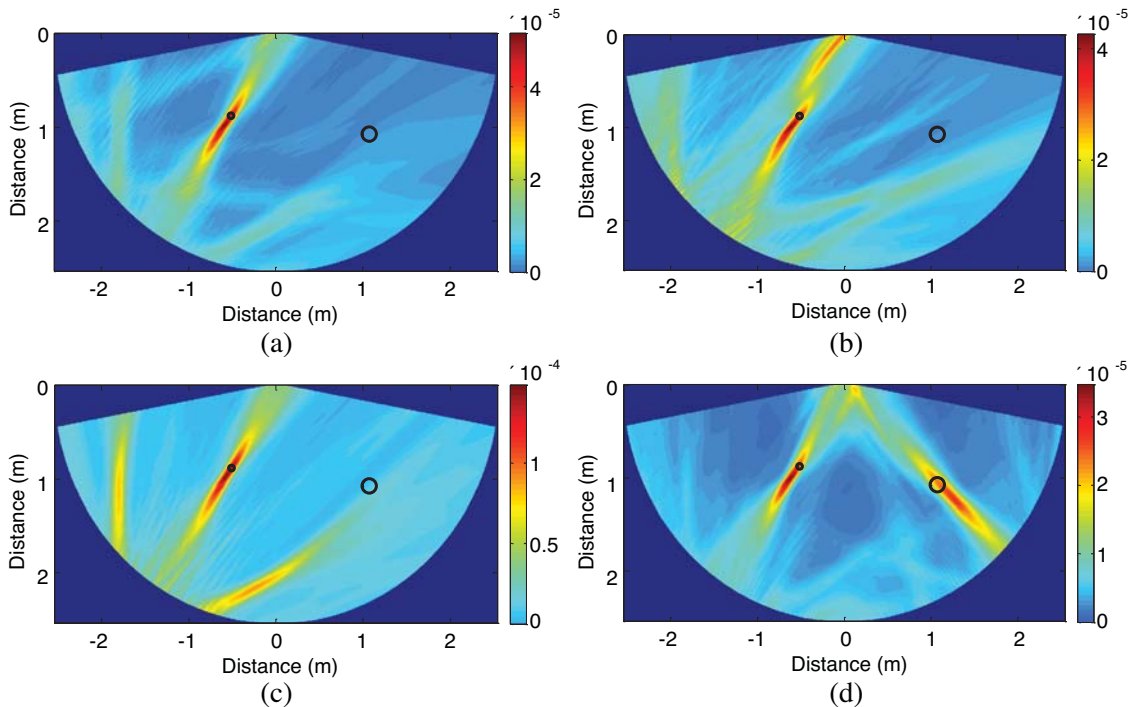
$$\epsilon = \frac{|\vec{r}_{det} - \vec{r}_{act}|}{r_{roi}}, \quad (3)$$

where \vec{r}_{det} is the highest intensity point in the image, \vec{r}_{act} the actual location of the dielectric center and r_{roi} the radius of the ROI which is equal to 100 inches. Table 1 shows the detection error calculated for different target positions. The results indicate that the error increases as the target moves away from the reflectarray. When the target is close to the array the error is less than 1%, however, it increases to about 9% when the target is located at 80" from the center.

The second experiment was designed to demonstrate the beam scanning ability of the system. Two cylindrical dielectrics with diameters of 2.25 and 6 inches were located at $(r, \theta) = (40'', -30^\circ)$ and $(r, \theta) = (60'', 45^\circ)$, respectively. The cylinders were both 3 feet long and made of acetal. In order to scan the region of interest, the beam was steered into various angles, starting from -60° to $+60^\circ$ in 15-degree increments, excluding $\pm 15^\circ$ due to the large profile of the lenses (see Section 2). At each steering angle the scattered field was measured along the arch rail. Similar to the previous experiment, the field was time-reversed and re-radiated back into the medium using computer simulation. Finally

Table 1. Detection error calculated for different positions of the dielectric cylinder.

Target distance from reflectarray (inch)	Detection error (ϵ)
40	9.4e-04
60	0.0471
80	0.0933



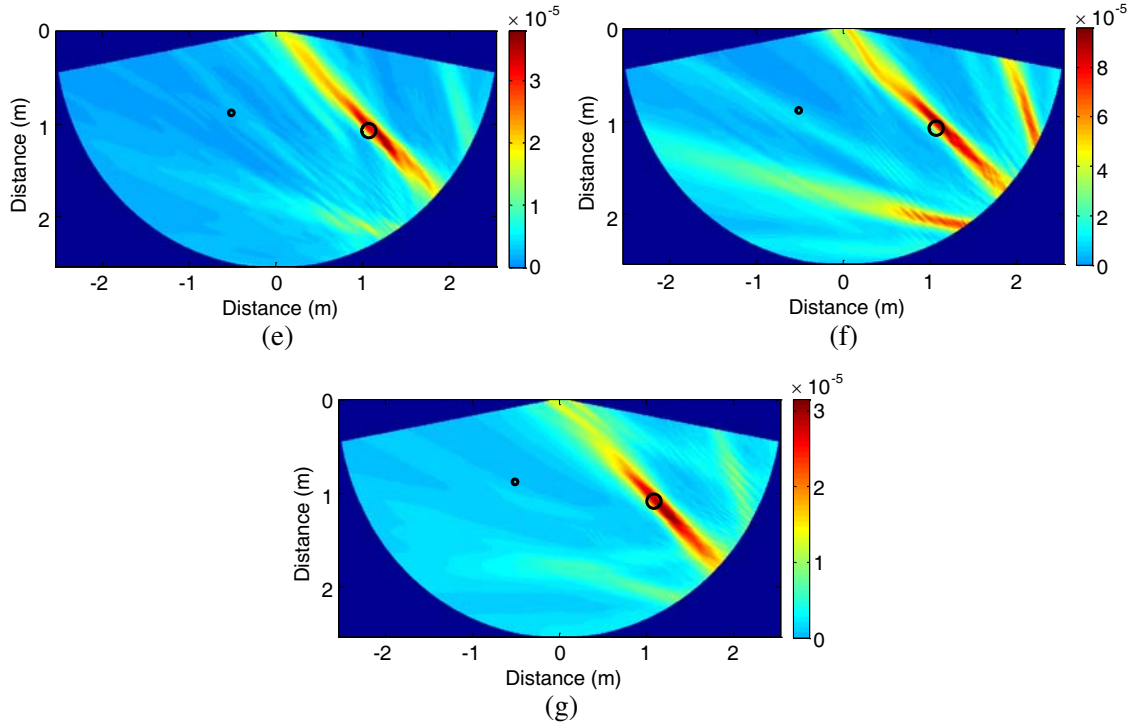


Figure 7. Experiment two. Energy image for different steering angles. The black circles correspond to the actual positions of the scatterers. (a) Beam steered to -60° . (b) Beam steered to -45° . (c) Beam steered to -30° . (d) Beam steered to 0° . (e) Beam steered to $+30^\circ$. (f) Beam steered to $+45^\circ$. (g) Beam steered to $+60^\circ$.

Table 2. Detection error calculated for different steering angles. ND indicates that the target was not detectable at the particular steering angle.

Steering angle (degree)	Detection error (ϵ) 2.25" diameter cylinder	Detection error (ϵ) 6.0" diameter cylinder
-60	0.0535	ND
-45	0.0592	ND
-30	0.0505	ND
0	0.0699	0.1046
30	ND	0.0565
45	ND	0.0401
60	ND	0.1141

the energy image was plotted in order to detect and locate the scatterers in the ROI. The results are shown in Fig. 7. The beam is steered to -60° and -45° , corresponding to Fig. 7(a) and Fig. 7(b), respectively. In both cases, the target located at $(r, \theta) = (40'', -30^\circ)$ is detected. This is due to the side lobes of the reflectarray (see Fig. 4). Fig. 7(c) shows the case where the main beam is steered to -30° and consequently passes through the target. In this case the interaction is maximized and hence, compared to the two previous cases, the target has a much stronger indication in the energy image. Similar to the first experiment, in case of maximum interaction, artifacts are more visible in the image. Fig. 7(d) corresponds to the case where the beam is reflected to 0° . In this case, both scatterers are detected. In the last three cases, where the main beam is deflected into $+30^\circ$, $+45^\circ$ and $+60^\circ$, only the bigger dielectric cylinder located at $(r, \theta) = (60'', +45^\circ)$ is detected. However, the strongest indication

of the target appears when the beam is steered to $+45^\circ$ which also results in stronger artifacts in the energy image.

In order to evaluate the accuracy of detection when the beam is steered into different angles, the relative error is calculated (see Table 2). As expected, the error is at a minimum (equal to or below 5%) when the main beam passes through the object and increases otherwise. Tables 1 and 2 indicate that detection error is smaller for larger scatterers due to a bigger scattered field. In addition, the error decreases for targets closer to the reflectarray. This is due to a more focused beam in closer proximity to the array.

5. CONCLUSION

A novel microwave imaging system is proposed in this paper. The primary component of the system is a tunable reflectarray antenna with high beam steering capabilities. This allows for the utilization of a single source which greatly reduces complexity and manufacturing cost. A prototype of this system was built and experimentally verified. Using the time reversal signal processing technique, the system was able to detect and locate cylindrical targets of different sizes and positions.

While the prototype was used in a 2-D setup, it can be readily extended to 3-D applications. This is possible by three dimensional beam steering of the reflectarray antenna, which can be achieved by controlling individual unit cells of the array as opposed to entire columns in the two dimensional case. Another area to explore is to recreate scatterer profiles in addition to detection. This would require more advanced reconstruction algorithms such as limited angle tomographic techniques [30–32]. Moreover, as the system is scalable, it has a range of potential applications such as medical imaging, defect detection in extended composite materials, etc. These are left for future studies.

REFERENCES

1. Bindu, G. N., S. J. Abraham, A. Lonappan, V. Thomas, C. K. Aanandan, and K. T. Mathew, "Active microwave imaging for breast cancer detection," *Progress In Electromagnetics Research*, Vol. 58, 149–169, 2006.
2. Liu, Z., H. Ukida, P. Ramuhalli, and K. Niel, *Integrated Imaging and Vision Techniques for Industrial Inspection*, Springer, 2015.
3. *Cancer Facts & Figures*, American Cancer Society, Inc., Atlanta, GA, 2015.
4. Fear, E. C., P. M. Meaney, and M. A. Stuchly, "Microwaves for breast cancer?," *IEEE Potentials*, Vol. 22, No. 1, 12–18, 2003.
5. Kharkovsky, S. and R. Zoughi, "Microwave and millimeter wave nondestructive testing and evaluation — Overview and recent advances," *IEEE Instrum. Meas. Mag.*, Vol. 10, No. 2, 26–38, 2007.
6. Meaney, P. M., M. W. Fanning, D. Li, S. P. Poplack, and K. D. Paulsen, "A clinical prototype for active microwave imaging of the breast," *IEEE Trans. Microw. Theory Techn.*, Vol. 48, No. 11, 1805–1808, 2000.
7. Qing, A. and C. K. Lee, "Microwave imaging of parallel perfectly conducting cylinders using real-coded genetic algorithm coupled with Newton-Kantorivitch method," *Progress In Electromagnetics Research*, Vol. 28, 275–294, 2000.
8. Golnabi, A. H., P. M. Meaney, S. D. Geimer, and K. D. Paulsen, "Comparison of no-prior and soft-prior regularization in biomedical microwave imaging," *J. Med. Phys.*, Vol. 36, 159–170, 2011.
9. Ostadrahimi, M., P. Mojtabai, S. Noghianian, J. LoVetri, and L. Shafai, "A multiprobe-per-collector modulated scatterer technique for microwave tomography," *IEEE Antennas Wireless Propag. Lett.*, Vol. 10, 1445–1448, 2011.
10. Gilmore, C., A. Zakaria, S. Pistorius, and J. LoVetri, "Microwave imaging of human forearms: Pilot study and image enhancement," *Int. J. Biomed. Imaging*, Vol. 2013, 673027, 2013.
11. Epstein, N. R., P. M. Meaney, and K. D. Paulsen, "3D parallel-detection microwave tomography for clinical breast imaging," *Rev. Sci. Instrum.*, Vol. 85, 124704, 2014.

12. Arunachalam, K., L. Udpa, and S. Udpa, "Microwave imaging of penetrable scatterers using deformable mirror," *IEEE Trans. Magn.*, Vol. 43, No. 4, 1805–1808, 2007.
13. Arunachalam, K., L. Udpa, and S. Udpa, "A computational investigation of microwave breast imaging using deformable reflector," *IEEE Trans. Biomed. Eng.*, Vol. 55, No. 2, 554–562, 2008.
14. Huang, J. and J. A. Enicar, *Reflectarray Antennas*, Wiley-IEEE Press, New Jersey, 2007.
15. Hum, S. V. and J. Perruissea-Carrier, "Reconfigurable reflectarrays and array lenses for dynamic antenna beam control: A review," *IEEE Trans. Antennas Propag.*, Vol. 62, No. 1, 183–198, 2014.
16. Nayeri, P., F. Yang, and A. Z. Elsherbani, "Beam-scanning reflectarray antennas: A technical overview and state of the art," *IEEE Antennas Propag. Mag.*, Vol. 57, No. 4, 32–47, 2015.
17. Tang, J., A. Tayebi, S. Udpa, E. J. Rothwell, and A. Temme, "A dual-band tunable reflectarray," *Proc. Int. Symp. Antennas Propag.*, 1033–1034, 2014.
18. Tayebi, A., J. Tang, P. Roy Paladhi, L. Udpa, and S. S. Udpa, "Design and development of an electrically-controlled beam steering mirror for microwave tomography," *AIP Conf. Proc.*, Vol. 1650, 501–508, 2015.
19. Tayebi, A., J. Tang, P. Roy Paladhi, L. Udpa, S. S. Udpa, and E. J. Rothwell, "Dynamic beam shaping using a dual-band electronically tunable reflectarray antenna," *IEEE Trans. Antennas Propag.*, Vol. 63, No. 10, 4534–4539, 2015.
20. Zubir, F., M. K. Abd Rahim, O. B. Ayop, and H. A. Majid, "Design and analysis of microstrip reflectarray antenna with minkowski shape radiating element," *Progress In Electromagnetics Research B*, Vol. 24, 317–331, 2010.
21. Perry, B. T., E. J. Rothwell, and L. C. Kempel, "A comparison of the measured pulse response of layered materials using time- and frequency-domain systems," *IEEE Antennas Propag. Mag.*, Vol. 49, No. 5, 117–123, 2007.
22. Bellomo, L., S. Pioch, M. Saillard, and E. Spano, "Time reversal experiments in the microwave range: Description of the radar and results," *Progress In Electromagnetics Research*, Vol. 104, 427–448, 2010.
23. Zhang, W., A. Hoorfar, and L. Li, "Through-the-wall target localization with time reversal MUSIC method," *Progress In Electromagnetics Research*, Vol. 106, 75–89, 2010.
24. Razavian, M., M. H. Hosseini, and R. Safian, "Time-reversal microwave imaging based on random configuration of transmitters or receivers," *Progress In Electromagnetics Research B*, Vol. 56, 235–250, 2013.
25. Kosmas, P. and M. Rappaport, "Time reversal with FDTD method for microwave breast cancer detection," *IEEE Trans. Microw. Theory Techn.*, Vol. 49, No. 7, 2317–2323, 2005.
26. Reyes-Rodríguez, S., N. Lei, B. Crowgey, L. Udpa, and S. S. Udpa, "Time reversal and microwave techniques for solving inverse problem in non-destructive evaluation," *NDT & E Int.*, Vol. 62, 106–114, 2014.
27. El Sahmarany, L., L. Berry, N. Ravot, F. Auzanneau, and P. Bonnet, "Time reversal for soft faults diagnosis in wire networks," *Progress In Electromagnetics Research M*, Vol. 31, 45–58, 2013.
28. Maaref, N., P. Millot, X. Ferrières, C. Pichot, and O. Picon, "Electromagnetic imaging method based on time reversal processing applied to through-the-wall target localization," *Progress In Electromagnetics Research M*, Vol. 1, 59–67, 2008.
29. Riddle, B., J. Baker-Jarvis, and J. Krupka, "Complex permittivity measurements of common plastics over variable temperatures," *IEEE Trans. Microw. Theory Techn.*, Vol. 51, No. 3, 727–733, 2003.
30. Roy Paladhi, P., A. Sinha, A. Tayebi, L. Udpa, and S. Udpa, "Class of backpropagation techniques for limited-angle reconstruction in microwave tomography," *AIP Conf. Proc.*, Vol. 1650, 509–518, 2015.
31. Roy Paladhi, P., A. K. Sinha, A. Tayebi, L. Udpa, and A. Tamburrino, "Data redundancy in diffraction tomography," *Int. Rev. Prog. Appl. Comput. Electrom. (ACES)*, 1–2, 2015.
32. Roy Paladhi, P., A. K. Sinha, A. Tayebi, L. Udpa, and S. S. Udpa, "Improved backpropagation algorithms by exploiting data redundancy in limited-angle diffraction tomography," *Progress In Electromagnetics Research B*, Vol. 66, 1–13, 2016.